

Electrically active point defects in Mg implanted n-type GaN grown by metal-organic chemical vapor deposition

G. Alfieri, V. K. Sundaramoorthy, and R. Micheletto

Citation: *Journal of Applied Physics* **123**, 205303 (2018); doi: 10.1063/1.5029254

View online: <https://doi.org/10.1063/1.5029254>

View Table of Contents: <http://aip.scitation.org/toc/jap/123/20>

Published by the American Institute of Physics

Articles you may be interested in

Geometric contribution leading to anomalous estimation of two-dimensional electron gas density in GaN based heterostructures

Journal of Applied Physics **123**, 205702 (2018); 10.1063/1.5026167

Large electron capture-cross-section of the major nonradiative recombination centers in Mg-doped GaN epilayers grown on a GaN substrate

Applied Physics Letters **112**, 211901 (2018); 10.1063/1.5030645

CdCl₂ passivation of polycrystalline CdMgTe and CdZnTe absorbers for tandem photovoltaic cells

Journal of Applied Physics **123**, 203101 (2018); 10.1063/1.5023811

Correlation between dislocations and leakage current of p-n diodes on a free-standing GaN substrate

Applied Physics Letters **112**, 182106 (2018); 10.1063/1.5024704

On compensation in Si-doped AlN

Applied Physics Letters **112**, 152101 (2018); 10.1063/1.5022794

Significant improvement in the electrical characteristics of Schottky barrier diodes on molecularly modified Gallium Nitride surfaces

Applied Physics Letters **112**, 163502 (2018); 10.1063/1.5005587

PHYSICS TODAY

WHITEPAPERS

MANAGER'S GUIDE

READ NOW

Accelerate R&D with
Multiphysics Simulation

PRESENTED BY
 COMSOL

Electrically active point defects in Mg implanted n-type GaN grown by metal-organic chemical vapor deposition

G. Alfieri,¹ V. K. Sundaramoorthy,¹ and R. Micheletto²

¹ABB Corporate Research, Segelhofstrasse 1K, 5405 Baden-Dättwil, Switzerland

²Department of Nanosystem Sciences, Yokohama City University, 236-0027 Yokohama, Japan

(Received 12 March 2018; accepted 10 May 2018; published online 24 May 2018)

Magnesium (Mg) is the *p*-type doping of choice for GaN, and selective area doping by ion implantation is a routine technique employed during device processing. While electrically active defects have been thoroughly studied in as-grown GaN, not much is known about defects generated by ion implantation. This is especially true for the case of Mg. In this study, we carried out an electrical characterization investigation of point defects generated by Mg implantation in GaN. We have found at least nine electrically active levels in the 0.2–1.2 eV energy range, below the conduction band. The isochronal annealing behavior of these levels showed that most of them are thermally stable up to 1000 °C. The nature of the detected defects is then discussed in the light of the results found in the literature. Published by AIP Publishing. <https://doi.org/10.1063/1.5029254>

I. INTRODUCTION

While *n*-type conductivity in GaN can be routinely achieved by Si-doping, *p*-type doping efficiency is still an issue. Magnesium is typically employed for *p*-type doping, and it is incorporated during growth. Mg occupies a Ga-site (Mg_{Ga}) and gives rise to an acceptor level at ~0.2 eV above the valence band edge (E_V).^{1,2} The reported activation ratio is 1%–2%,^{3,4} meaning that high concentrations of Mg must be incorporated into GaN in order to obtain, at room temperature, a hole concentration that is acceptable for device applications. To complicate matters even further, H passivation, as well as compensation due to nitrogen vacancies (V_N)⁵ and Mg interstitials (Mg_i),¹ must be taken into account when dealing with Mg doped GaN.

Selective area doping is a common process in semiconductor device manufacturing for the formation of p^+ regions, and GaN devices are no exception.^{6,7} It is known that ion implantation leads to the formation of point defects which can give rise to electrically active levels. Electrically active point defects can undermine the correct functionality of the device, which is why post-implantation heat treatments are required to anneal out such defects. For device processing, p^+ regions are formed by multiple ion implantation (box-profile implantation) and such defects are also found at the implantation tail of the box-profile where concentrations as high as 10^{15} cm^{-3} have been reported.⁸

Positron annihilation spectroscopy (PAS) studies⁹ have shown that V_N and gallium vacancies (V_{Ga}), formed after Mg implantation, form clusters $[(V_{Ga})_n V_N]$ after annealing at 1000 °C. However, Lardeau-Falcy *et al.*¹⁰ have shown that an annealing temperature of at least 1000 °C is necessary to remove the presence of point defects generated by ion implantation. Recent investigations on Mg implanted GaN have reported that the density of deep levels was reduced after annealing at 800 °C.⁹ Nevertheless, devices that underwent annealing at 1400 °C, with the use of AlN capping, showed a rather low breakdown voltage (~300 V) despite

the thickness of the drift layer (10 μm). One of the causes was attributed to the presence of a highly defective layer at the junction.⁷

As evident from the above-mentioned literature, despite the technological importance of Mg implantation for GaN power devices, it is still not known what electrically active defects arise after Mg implantation and how thermally stable these defects are. In order to shed light on this topic, we present an electrical characterization and isochronal annealing study of Mg implanted GaN.

II. EXPERIMENTAL DETAILS

1 μm thick Si-doped GaN epilayers (net donor concentration, N_d , $3\text{--}5 \times 10^{16} \text{ cm}^{-3}$, $[C] \sim 1 \times 10^{16} \text{ cm}^{-3}$) grown by metal-organic chemical vapor deposition (MOCVD) on GaN substrates were purchased from NTT (Japan). Samples were cleaned by a mixture of $H_2O:HCl$, and after being rinsed with deionized water, a Ti/Al (40/150 nm) bilayer was deposited on the backside. Rapid thermal annealing (RTA) for 5 min at 550 °C leads to the formation of ohmic contacts. Samples were then implanted with 200 keV Mg ions and a dose of 10^{11} cm^{-2} , at room temperature. This dose, which is low for device fabrication, was chosen in order that the implanted region could simulate the implant tail region of a box-profile. For this reason, GaN epilayers have retained their original *n*-type conductivity. After implantation, Schottky contacts were formed by e-beam deposition of Ni (70 nm) on the frontside of the samples.

Electrical characterization was carried out by capacitance voltage (C-V) and Fourier-transform deep level transient spectroscopy (FT-DLTS).¹¹ The reverse bias (V_r) for FT-DLTS measurements was set to -5 V, to cover the implantation profile, pulsed to 0 V by employing a filling pulse of 1 ms and a period width of 0.2 s. FT-DLTS was performed in the 100–650 K temperature range, always starting from 100 K.

An isochronal annealing study of the electrically active traps was performed between 100 and 1000 °C, with a time step of 1 min, by using RTA in vacuum. This choice was motivated by the fact that RTA treated Mg doped GaN leads to a similar hole concentration, like a traditional furnace, but has higher hole mobility.¹² For samples annealed up to 400 °C, the highest measurement temperature coincided with the annealing temperature. Heat treatments from 600 °C were performed by first removing the Ni metal contacts by *aqua regia* and the Ti/Al bilayer by HF 5% aqueous solution.

III. RESULTS AND DISCUSSION

Figure 1(a) displays the Mg implantation profile and the vacancy concentrations obtained by full-cascades Monte Carlo simulations.¹³ The displacement energies of Ga and N are 39 eV and 17 eV, respectively.¹⁴ In Fig. 1(a), N_d , obtained by C-V measurements on the as-grown and implanted samples, is also shown. As can be seen, the Mg implantation profile has a maximum concentration of $\sim 4 \times 10^{15} \text{ cm}^{-3}$ at $\sim 0.25 \mu\text{m}$, while the concentrations of both V_{Ga} and V_N are almost three orders of magnitude higher.

After implantation, the N_d profile is detected beyond the implanted Mg profile, at a depth of 0.5–0.6 μm . After annealing at 300 °C, N_d is slightly changed, but only after annealing at 400 °C, N_d is reactivated near the implanted area. Annealing at 500 °C results in the recovery of N_d to the as-grown conditions. This is more evident after heat treatments at 800 °C.

The reason why N_d is only detected outside the implanted area, after implantation, can be explained in terms of formation of compensating centers. Figure 1(b) shows $1/C^2$ versus V_r for the as-grown, as-implanted, and annealed samples. As it can be seen, the $C^{-2}-V_r$ relationship, for the as-grown sample, is linear in agreement with the uniform N_d distribution over the studied depth range. After implantation, the capacitance is reduced and $C^{-2}-V_r$ is not linear anymore. As a matter of fact, close to the surface (low V_r), the capacitance is independent of

the voltage, suggesting that implantation leads to a compensated layer. This layer is gradually removed by annealing (≥ 500 °C), and the linearity of $C^{-2}-V_r$ is restored meaning that the compensating species are either annealed out or diffuse in the bulk. Interestingly, the temperature (500 °C) at which N_d approaches the as-grown profile (or $C^{-2}-V_r$ becomes linear) is the same temperature at which the electron paramagnetic resonance (EPR) signal of V_{Ga} was reported to anneal out.¹⁵ Furthermore, it was recently reported that at ≥ 500 °C, the carrier concentration of Mg implanted metal-organic vapor phase epitaxy (MOVPE) GaN recovers to the as-grown levels.¹⁶

In order to identify those defects responsible for compensation, Saarinen *et al.*¹⁷ have shown that V_{Ga} is the main compensating center in N-rich MOCVD GaN. This is also confirmed by theory that predicts a lower formation energy of the single negative charge state of V_{Ga} in N-rich rather than Ga-rich conditions.¹⁸ However, its formation energy is positive (~ 2.5 eV) and this makes $[V_{Ga}]$ limited. For this reason, it can be thought that it is not V_{Ga} alone the reason for carrier compensation but rather V_{Ga} jointly to other defects, such as interstitials, antisites, or V_{Ga} -related complexes.

Ga or N antisites (Ga_N and N_{Ga}) or even N interstitials (N_i) and V_{Ga} behave as acceptors in *n*-type GaN.⁵ However, the formation energy of antisites and interstitials is so high (≥ 5 eV), in *n*-type GaN, that their concentration is negligible. It can be thought that divacancies ($V_{Ga}V_N$) can form after implantation. These behave as acceptors.¹⁹ However, PAS measurements⁹ on Mg implanted GaN have shown that $V_{Ga}V_N$ forms only after high temperature heat treatments (1000 °C). $V_{Ga}(V_N)_2$ were found after implantation,⁹ but nothing is known about their donor/acceptor nature. Carbon, which is also present in high concentrations in our samples, can also form complexes with either V_{Ga} or V_N , but such complexes possess very high formation energies.²⁰ A more plausible hypothesis would be the formation of Si-related complexes. As a matter of fact, it was shown that a V_{Ga} -complex, formed with Si, gives rise to an acceptor in

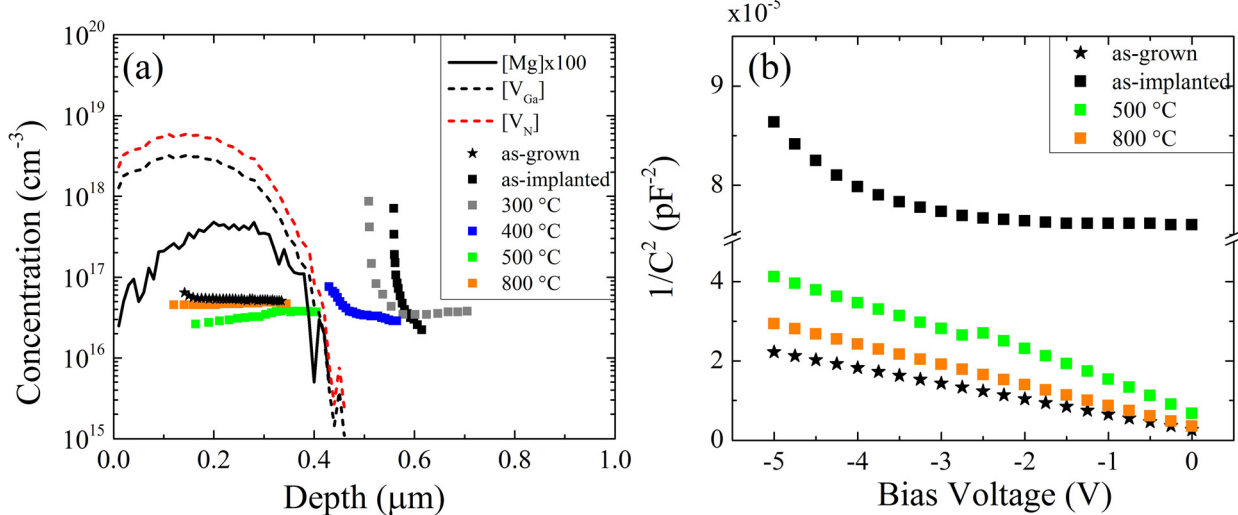


FIG. 1. (a) Simulated Mg and V_{Ga} , V_N profiles, as obtained by SRIM (solid/dashed lines). This is plotted together with the net-donor profiles in the as-grown, as-implanted, implanted, and annealed GaN epilayers, at 300, 400, 500, and 800 °C (squares). The Mg implanted profile was multiplied by a factor of 100, for clarity. (b) Measured $C^{-2}-V_r$ characteristics for the as-grown, as-implanted, and 500 and 800 °C annealed samples.

n-type GaN and has a negative formation energy²¹ meaning that it can be very abundant in *n*-type GaN.

Figure 2 shows the DLTS spectra of the as-grown, as-implanted, and annealed GaN epilayers. In the as-grown MOCVD GaN [Fig. 2(a)], two traps are found at 0.20 and 0.56 eV below the conduction band edge (E_C) and labeled M1 and M2, respectively. M1 has a concentration of 10^{13} cm^{-3} and a capture cross section of 10^{-16} cm^2 , while M2 has a concentration of $4.2 \times 10^{14} \text{ cm}^{-3}$ and a capture cross section of $1.5 \times 10^{-16} \text{ cm}^2$. In addition, although not shown here, annealing the as-grown sample at higher temperatures ($>500^\circ\text{C}$) also revealed the presence of only M1 and M2. After implantation [Fig. 2(a)], another level is found, labeled M3, at $E_C - 0.63 \text{ eV}$ ($6 \times 10^{17} \text{ cm}^{-3}$ and $3.5 \times 10^{-16} \text{ cm}^2$). It is interesting to note that the M1 level is not detected after implantation. Annealing at 300°C [Fig. 2(b)] leads to the formation of another level, M4 ($E_C - 0.70 \text{ eV}$, $1 \times 10^{16} \text{ cm}^{-3}$, and 10^{-14} cm^2). The DLTS peak labeled M4 spans on a temperature range of $\sim 200 \text{ K}$, meaning that it may be formed by the overlapping of different contributions, e.g., the M3 level. In order to uncover such contributions, we applied the following:¹¹

$$S = \frac{N_T C_{st}}{T_W N_D} (e^{-T_W/\tau} - 1) \frac{2\pi/T_W}{1/\tau^2 + (2\pi/T_W)^2}, \quad (1)$$

where N_T , C_{st} , and T_W are the trap concentration, the steady capacitance under the reverse bias condition, and the period width, respectively, while $\tau = \frac{1}{\sigma v_{th} N_C} e^{E_C - E_T / kT}$ with σ , v_{th} , N_C , E_T , and k being the capture cross section, thermal velocity, effective density of states, activation energy, and Boltzmann constant, respectively.

Figure 2(b) shows that the sum (red solid line) of the M3 and M4* ($E_C - 0.69 \text{ eV}$ and $3.8 \times 10^{-16} \text{ cm}^2$) levels (red dashed lines), obtained by using Eq. (1), reproduces the M4 DLTS signal quite well. Subsequent heat treatments at 400°C [Fig. 2(c)] reveal the presence of a broader DLTS peak. This peak is labeled M5 ($E_C - 0.68 \text{ eV}$, $1.3 \times 10^{16} \text{ cm}^{-3}$, and 10^{-16} cm^2) and it is too broad to be assigned to a single level.

Being this DLTS peak wider than that found after annealing at 300°C ($\sim 250 \text{ K}$ wide) means that it may be due to the overlapping of the M4 DLTS peak and other contributions. We subtracted the two DLTS signals detected after 400 and 300°C . The result is shown as white circles in Fig. 2(c). By using Eq. (1), it can be seen that this peak is given by the sum (solid red line) of two DLTS peaks, M5* and M5**, located at $E_C - 0.65 \text{ eV}$ and $E_C - 0.72 \text{ eV}$, respectively (dashed red lines).

In Fig. 2(d), the DLTS spectrum of the Mg implanted GaN annealed at 500°C is shown. Besides the M1 level, the M4 is also clearly detectable. A new level is found at $\sim 230 \text{ K}$ and labeled M6 ($E_C - 0.51 \text{ eV}$, $5 \times 10^{14} \text{ cm}^{-3}$, and $7 \times 10^{-14} \text{ cm}^2$). A shoulder peak is found at $\sim 400 \text{ K}$, but the estimation of its energy position in the bandgap is rather difficult at this stage, and another peak, at $\sim 440 \text{ K}$, labeled M7, is detected. The latter has the same temperature position of the M5** peak obtained by our fitting, so they may be assigned to the same level ($E_C - 0.75 \text{ eV}$, $2.4 \times 10^{15} \text{ cm}^{-3}$, and $1 \times 10^{-16} \text{ cm}^2$). At $\sim 540 \text{ K}$, a peak labeled M8 is assigned to a level located at $E_C - 1.2 \text{ eV}$ ($6 \times 10^{14} \text{ cm}^{-3}$ and $5 \times 10^{-15} \text{ cm}^2$). After annealing at 800°C [Fig. 2(e)], the M1, M6, M4, and M8 levels are still present. In addition, the previously detected shoulder peak is now more clearly visible and labeled M9 ($E_C - 0.67 \text{ eV}$, $1 \times 10^{15} \text{ cm}^{-3}$, $2 \times 10^{-15} \text{ cm}^2$). Similar to the case of M7 (which is annealed out at this stage), the M9 temperature peak position is like that of M5*. For this reason, they may be assigned to the same electrically active level.

The last annealing stage [Fig. 2(f)] shows that M1 ($1.1 \times 10^{16} \text{ cm}^{-3}$), M6 ($2.6 \times 10^{14} \text{ cm}^{-3}$), M4 ($5 \times 10^{14} \text{ cm}^{-3}$), M8 ($2 \times 10^{15} \text{ cm}^{-3}$), and M9 ($7 \times 10^{14} \text{ cm}^{-3}$) are still persistent. We can also detect a peak which was earlier assigned to the M2 level ($4 \times 10^{14} \text{ cm}^{-3}$), found in the as-grown material. All the detected trap did not show electric field dependence, suggesting that they are of acceptor type. A summary of the detected traps is reported in Table I.

The trap M1 has been detected in GaN grown by MOCVD,^{22–24} molecular beam epitaxy (MBE),²⁵ and halide

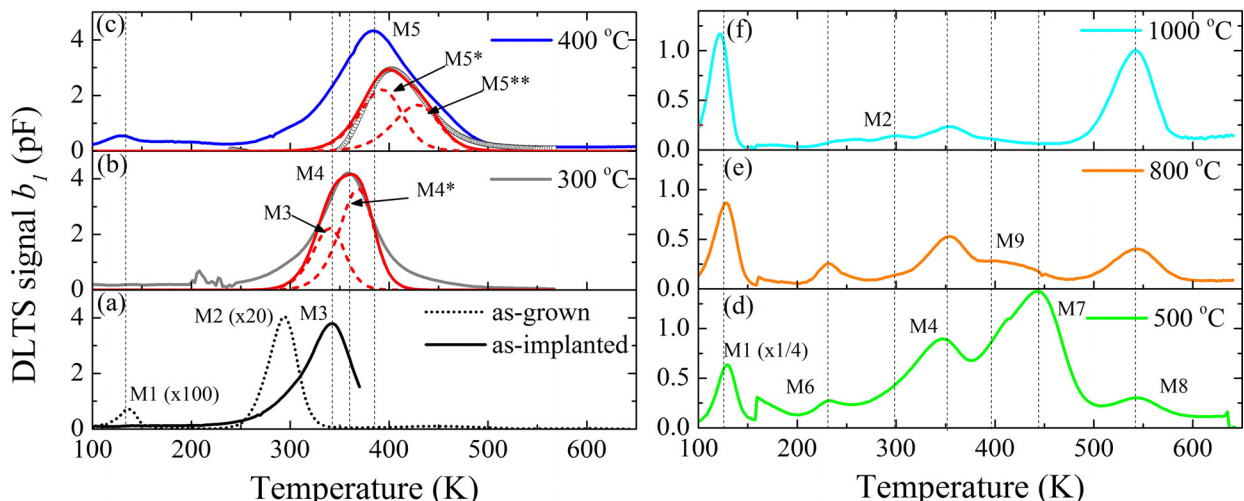


FIG. 2. DLTS spectra of the (a) as-grown and as-implanted, (b) 300°C , (c) 400°C , (d) 500°C , (e) 800°C , and (f) 1000°C annealed samples. White dots represent the difference between two DLTS signals whereas red and dashed solid lines represent the analytical fit of the DLTS peaks. The period width is set to 0.2 s for all measurements.

TABLE I. Labeling, energy position in the bandgap (eV), capture cross section (cm^2), and conditions for detection of the levels found in this study.

Label	$E_C - E_T$ (eV)	Capture cross section (cm^2)	Comment
M1	0.20 ± 0.01	$(1 \pm 0.03) \times 10^{-16}$	In as-grown and implanted materials
M2	0.56 ± 0.01	$(1.50 \pm 0.04) \times 10^{-16}$	Found in the as-grown material
M3	0.63 ± 0.02	$(3.5 \pm 0.1) \times 10^{-16}$	Found in the as-implanted material
M4	0.70 ± 0.01	$(1 \pm 0.02) \times 10^{-16}$	Stable up to 1000°C
M5	0.68 ± 0.01	$(1.6 \pm 0.08) \times 10^{-16}$	Detected after 400°C
M6	0.51 ± 0.01	$(5 \pm 0.05) \times 10^{-14}$	Detected after 300°C
M7	0.75 ± 0.01	$(1 \pm 0.1) \times 10^{-16}$	Same as M5**. Anneals out at 800°C
M8	1.12 ± 0.02	$(5 \pm 0.1) \times 10^{-15}$	Found after 500°C . Stable up to 1000°C
M9	0.67 ± 0.03	$(2 \pm 0.2) \times 10^{-15}$	Same as M5*. Stable up to 1000°C

vapor phase epitaxy (HVPE)-grown material²⁶ and labeled in different ways, in the past. Its nature has been attributed to either a divacancy (V_NV_{Ga}) or an impurity related complex.²⁷ We observe that, despite being present in the as-grown material, M1 cannot be detected right after implantation, when N_d is detected away from the implanted region. However, it can be found again after annealing at 400°C and, for subsequent annealing steps, the M1 is always present with a rather constant concentration. If M1 were related to a divacancy, it would be reasonable to expect an increase in the concentration for subsequent annealing steps, e.g., when N_d is reactivated inside the implanted area. Recent hybrid density functional calculation (DFT) showed that divacancies in GaN form acceptors much deeper than $E_C - 0.20\text{ eV}$.¹⁹ For these reasons, the hypothesis of an impurity (C or H)-related complex might be favored. As a matter of fact, a DFT study performed by Matsubara and Bellotti²⁰ reported a level at $E_C - 0.22\text{ eV}$ for the C_{Ga}V_N complex.

Similar to M1, M2 has also been detected in GaN grown by MOCVD^{22–24} and HVPE.²⁶ In the present study, the M2 level is detected in the as-grown material and in the implanted and 1000°C annealed samples. However, contrary to the case of M1, M2 might have been present at each annealing step with its signal buried under the broader M4 and M5 DLTS peaks. Furthermore, M2 is stable up to 1000°C in both electron irradiated GaN, where it was labeled D3²⁶ and, although not shown here, also in as-grown GaN. Regarding the microscopic structure of M2, N_{Ga} or a C-related defect has been suggested. Since this trap can also be found in HVPE grown GaN, where C contamination is absent, the former hypothesis seems to be more realistic.

The M3 level found after implantation is stable up to 1000°C . Chen *et al.*²⁴ have found an electron beam evaporation induced level, labeled E4, at $E_C - 0.65 - 0.70\text{ eV}$ close to the M3 level. In our investigation, metal contacts were also performed by electron-beam evaporation so it would be tempting to identify the M3 level as E4. However, the shape of E4 is much broader than that of M3 and we would expect to find E4 also in the as-grown material, which is not the

case. In addition, M3 is detected when the N_d profile is $>0.5\text{ }\mu\text{m}$ away from the surface. Another possibility would be the identification of M3 with the D3 level detected by Haase *et al.*²⁸ in N-implanted GaN. Similar to the D3 level, also M3 is found after implantation and it is thermally stable up to 900°C .

The energy position and thermal stability of the D4 level found in as-grown and electron irradiated HVPE grown GaN²⁶ are similar to those of the M4 level. However, the M4 level is not found in as-grown MOCVD GaN, meaning that its nature may be different from that of the D4 level. Polyakov *et al.*²⁹ have reported a level close to M4 in Cr implanted GaN and related it to a defect located in the implanted region. However, M4 is found after annealing at 300°C when N_d is away from the Mg-implanted area. This suggests that the level generated by Cr-implantation and the M4 level have a different microscopic structure. A similar argument holds for the M5 level, which is very close in energy position to the M4 level, resulting from the overlapping of several contributions, like the M4, M5*, and M5** levels.

Heat treatments at 500°C result in the formation of the M6 level. No data on this electrically active level have been reported in the literature. This, together with the facts that at this annealing stage the N_d is reactivated inside the Mg implanted area and that no significant diffusion of Mg occurs up to 1060°C ,³⁰ might suggest that the M6 level could be a Mg-related defect. However, DFT studies have shown that typically, Mg-related defects, such as Mg_i , Mg_{Ga}V_N , Mg_{Ga}H , and $\text{Mg}_{Ga}\text{V}_N\text{H}$, are either close to the valence band, rather than to the conduction band, or do not yield any level in the bandgap.^{1,31} Indeed, Duc *et al.*³² have found an acceptor trap in Mg-doped MOCVD-grown GaN at $E_V + 0.57 - 0.60\text{ eV}$ and assigned it to a Mg-related defect. In addition, Albrecht *et al.*³³ have not found any Mg-related defect in n-type GaN grown on sapphire implanted with the ^{28}Mg radio-active isotope and annealed at 1000°C , by radiotracer DLTS. In the present investigation, although the role of Mg cannot be completely ruled out, we find that the M6 level could possibly be identified as the E2 level detected in As-implanted and 800°C annealed GaN.³⁴ Another candidate for the identification of M6 could also be the oxygen-carbon complex which has been reported to be at $E_C - 0.57\text{ eV}$.³⁵

M7 is identified as M5** and this rules out the possibility of a Mg-related defect because, after annealing at 400°C , N_d is still detected outside the Mg-implanted region. The M7 level has a high thermal stability, similar to that of the D5I trap which is detected after electron irradiation.²⁶ Although M7 is 0.1 eV shallower than D5I, they might share a common microscopic nature which for the case of the D5I level was associated with an intrinsic defect.

Coming to the deepest level found in our study, the M8 level, we rule out the possibility that it can be identified as the D6 level.²⁶ This is because, contrary to D6, the M8 level has a higher thermal stability. Similar to the case of M6, also M8 is found when N_d reactivation is observed in the implanted area. Analogously, even if theory does not predict the presence of Mg-related defects close to E_C , the role of

Mg in the nature of the M8 level cannot be completely ruled out. Yet, Matsubara and Bellotti³⁵ have predicted that the $C_{NV_{Ga}}$ defect yields a level at $E_C - 1.16$ eV, very close to the M8 level. As M8 is found in a region where a high concentration of V_{Ga} is present and since C is a common impurity in MOCVD-grown GaN, we consider that this would be a possible candidate for the microscopic structure of the M8 level.

For the M9 level, similar considerations to the M7 level hold true. In fact, the M9 level shares a similar temperature position of the M5* level which suggests that they are indeed the same level. This means that the involvement of Mg in the nature of this level can be discarded. Further considerations on its nature cannot be put forward, due to the lack of data in the literature.

For most of the levels, the involvement of Mg in their microscopic structure can be ruled out, as they are detected when N_d is found outside the implanted region. However, this is not the case for M6 and M8. In light of this, we now focus our discussion on these two levels. Figure 3 shows the depth profile measurements performed on the 500 °C annealed sample, for M4, M6, and M8. The measurements were performed by varying V_r and keeping the pulse height constant. As the figure shows, the depth profiles of these three levels are located in the implanted region, in accordance with the behavior of N_d at this annealing stage. While M4 seems to possess a localized distribution at around $\sim 0.1 \mu\text{m}$, M6 and M8 display a steep profile toward the surface. In particular, M8 has a shallower profile than M6 and the absence of a localized profile around the implantation maximum suggests that Mg may not be involved in its atomic nature. On the other side, M6 also has a steep profile toward the surface but it is not possible to say, whether or not it is localized in the implanted region. If the profile keeps increasing toward the surface, then the involvement of Mg can be ruled out. However, if it shows a localized distribution inside the implanted region, then the involvement of Mg can be possible.

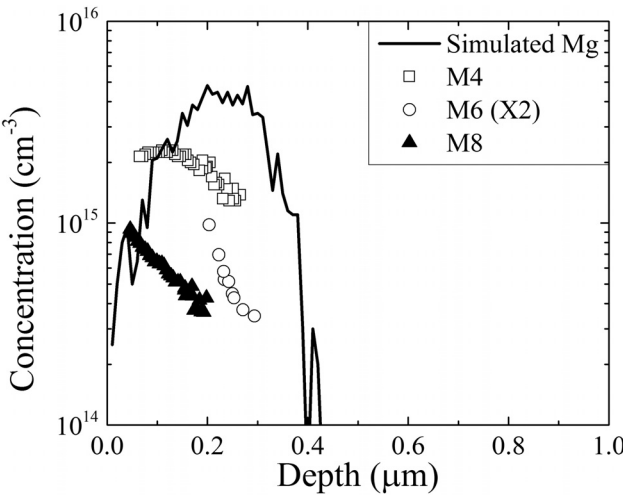


FIG. 3. Depth profile of the implanted Mg and of the M4, M6, and M8 levels. Depth profile measurements were carried out on the 500 °C annealed sample. The depth profile of M6 was increased to improve visualization. The Mg implantation profile was simulated by SRIM.

IV. CONCLUSIONS

Our study shows the presence of at least nine electrically active levels in Mg implanted GaN. These are located in the 0.2–1.2 eV energy range, below the conduction band edge, and their possible microscopic structure was discussed in the light of previous results found in the literature. The isochronal annealing study showed that M1, M2, M4, M6, M8, and M9 are thermally stable up to 1000 °C. In particular, after annealing at 1000 °C, two levels labeled M1 and M8, at $E_C - 0.22$ eV and $E_C - 1.12$ eV, respectively, are present with concentrations ranging between 10^{14} and 10^{16} cm^{-3} . This suggests that, when selective area doping is performed by ion implantation (e.g., box-profile), care should be taken to the deeper region of the implant profile (implant tail region) where such a defect could effectively trap charge carriers hindering the device functionality.

- ¹G. Miceli and A. Pasquarello, *Phys. Rev. B* **93**, 165207 (2016); and references therein.
- ²J. Lyons, A. Janotti, and C. G. van de Walle, *Phys. Rev. Lett.* **108**, 156403 (2012).
- ³T. Niwa, T. Fujii, and T. Oka, *Appl. Phys. Express* **10**, 091002 (2017).
- ⁴H. T. Chen, C. Y. Su, C. G. Tu, Y. F. Yao, C. H. Lin, Y. R. Wu, Y. W. Kiang, and C. C. Yang, *IEEE Trans. Electron Devices* **64**, 115 (2017).
- ⁵J. Lyons and C. G. van de Walle, *NPJ Comput. Mater.* **3**, 12 (2017).
- ⁶A. D. Koehler, T. J. Anderson, M. J. Tadjer, B. N. Feigelson, K. D. Hobart, F. J. Kub, A. Nath, and D. I. Shahin, in *Proceedings of the 2016 IEEE 4th Workshop on Wide Bandgap Power Devices and Applications (WiPDA)* (2016).
- ⁷D. Greenlee, T. J. Anderson, B. H. Feigelson, K. D. Hobart, and F. J. Kub, *Phys. Status Solidi A* **212**, 2772 (2015).
- ⁸Y. Negoro, T. Kimoto, and H. Matsunami, *J. Appl. Phys.* **98**, 043709 (2005).
- ⁹A. Uedono, S. Takashima, M. Edo, K. Ueno, H. Matsuyama, H. Kudo, H. Naramoto, and S. Ishibashi, *Phys. Status Solidi B* **252**, 2794 (2015).
- ¹⁰A. Lardeau-Falcy, M. Coig, M. Charles, C. Licitra, J. Kanyandekwe, F. Milesi, and J. Emery, in *Proceedings of the 232nd ECS Meeting* (2017).
- ¹¹S. Weiss and R. Kassing, *Solid-State Electron.* **31**, 1733 (1988).
- ¹²C. F. Lin, H. C. Cheng, C. C. Chang, and G. C. Chi, *J. Appl. Phys.* **88**, 6515 (2000).
- ¹³J. F. Ziegler *et al.*, *The Stopping and Range of Ions in Solids* (Pergamon, New York, 1985).
- ¹⁴H. Y. Xiao, F. Gao, X. T. Zu, and W. J. Weber, *J. Appl. Phys.* **105**, 123527 (2009).
- ¹⁵C. Bozdog, H. Przybylinska, G. D. Watkins, V. Härlé, F. Scholz, M. Mayer, M. Kamp, R. J. Molnar, A. E. Wickenden, D. D. Koleske, and R. L. Henry, *Phys. Rev. B* **59**, 12479 (1999).
- ¹⁶M. Akazawa, N. Yokota, and K. Uetake, *AIP Adv.* **8**, 025310 (2018).
- ¹⁷K. Saarinen, P. Seppälä, J. Oila, P. Hautojärvi, and C. Corbel, *Appl. Phys. Lett.* **73**, 3253 (1998).
- ¹⁸G. Miceli and A. Pasquarello, *Microelectron. Eng.* **147**, 51 (2015).
- ¹⁹I. C. Diallo, Ph.D. thesis, Virginia Commonwealth University, 2017.
- ²⁰M. Matsubara and E. Bellotti, *J. Appl. Phys.* **121**, 195701 (2017).
- ²¹I. C. Diallo, M.S. thesis, Virginia Commonwealth University, 2013.
- ²²Z. Q. Fang, D. C. Look, K. L. Wang, J. Han, F. A. Khan, and I. Adesida, *Appl. Phys. Lett.* **82**, 1562 (2003).
- ²³D. Johnstone, S. Dogan, J. Leach, Y. T. Moon, Y. Fu, Y. Hu, and H. Morkoc, *Appl. Phys. Lett.* **85**, 4058 (2004).
- ²⁴S. Chen, U. Honda, T. Shibata, T. Matsumura, Y. Tokuda, K. Ishikawa, M. Hori, H. Ueda, T. Uesugi, and T. Kachi, *J. Appl. Phys.* **112**, 053513 (2012).
- ²⁵L. Polenta, Z. Q. Fang, and D. C. Look, *Appl. Phys. Lett.* **76**, 2086 (2000).
- ²⁶T. T. Duc, G. Pozina, N. T. Son, E. Janzen, T. Ohshima, and C. Hemmingsson, *Appl. Phys. Lett.* **105**, 102103 (2014).
- ²⁷W. I. Lee, T. C. Huang, J. D. Guo, and M. S. Feng, *Appl. Phys. Lett.* **67**, 1721 (1995).
- ²⁸D. Haase, M. Schmid, W. Kürner, A. Dörnen, V. Härlé, F. Scholz, M. Buckard, and H. Schweizer, *Appl. Phys. Lett.* **69**, 2525 (1996).

- ²⁹A. Y. Polyakov, N. B. Smirnov, A. V. Govorkov, N. V. Pashkova, A. A. Shelensky, S. J. Pearton, M. E. Overberg, C. R. Abernathy, J. M. Zavada, and R. G. Wilson, *J. Appl. Phys.* **93**, 5388 (2003).
- ³⁰Y. L. Chang, M. Ludowise, D. Lefforge, and B. Perez, *Appl. Phys. Lett.* **74**, 688 (1999).
- ³¹C. Freysoldt, B. Lange, J. Neugebauer, Q. Yan, J. L. Lyons, A. Janotti, and C. G. van de Walle, *Phys. Rev. B* **93**, 165206 (2016); and references therein.
- ³²T. T. Duc, G. Pozina, H. Amano, B. Monemar, E. Janzen, and C. Hemmingsson, *Phys. Rev. B* **94**, 045206 (2016).
- ³³F. Albrecht, G. Pasold, J. Grillenberger, U. Reislöhner, M. Dietrich, and W. Witthuhn, *Mater. Sci. Forum* **457–460**, 1609 (2004).
- ³⁴L. Lee, W. C. Lee, H. M. Chung, M. C. Lee, W. H. Chen, W. K. Chen, and H. Y. Lee, *Appl. Phys. Lett.* **81**, 1812 (2002).
- ³⁵M. Matsubara and E. Bellotti, *J. Appl. Phys.* **121**, 195702 (2017).